

## Soft QCD measurements at LHC

M. Taševský\*

*On behalf of the ALICE, ATLAS, CMS,  
LHCb, LHCf and TOTEM collaborations*

*Institute of Physics of the Czech Academy of Sciences,  
Na Slovance 2, Prague, 18221, Czech Republic  
\*E-mail: Marek.Tasevsky@cern.ch*

Results from recent soft QCD measurements by LHC experiments ALICE, ATLAS, CMS, LHCb, LHCf and TOTEM are reported. The measurements include total, elastic and inelastic cross sections, inclusive and identified particle spectra, underlying event and hadronic chains. Results from particle correlations in all three collision systems, namely  $pp$ ,  $pPb$  and  $PbPb$ , exhibit unexpected similarities.

*Keywords:* soft QCD; total cross section; inclusive particle spectra; identified particle spectra; underlying event; particle correlations; hadronization

### 1. Introduction

Soft Quantum Chromodynamics (QCD) physics is a domain of particle physics which is characterized by a low momentum transfer, typically a low transverse momentum,  $p_T$ . It is usually used to describe that part of the scattering which dominates at soft scales and where perturbative QCD cannot be applied. One example of a process which is entirely governed by soft QCD physics is the process of hadronization. Since there is no uniform description of the phenomena that occur at low  $p_T$ , there is a variety of models trying to explain them through comparisons with extracted data. There is a wealth of LHC measurements that probe the soft QCD region — basically all LHC experiments measure soft QCD phenomena. This text reports on results from experiments ALICE<sup>1</sup>, ATLAS<sup>2</sup>, CMS<sup>3</sup>, LHCb<sup>4</sup>, LHCf<sup>5</sup> and TOTEM<sup>6</sup> and tries to select those which are recent and illustrative at the same time. We will discuss measurements of inclusive total cross sections, inclusive and identified particle spectra, underlying event, particle correlations and it will also be shown that there are surprising similarities between results from all three collision system:  $pp$ ,  $pPb$  and  $PbPb$  collisions. The models which will be occasionally mentioned are based on multi-parton interactions (MPI), color reconnections (CR), hadronization and hydrodynamical laws or gluon saturation in the proton. We will also see that there are very interesting links between three big domains of particle physics, namely particle collisions, heavy-ion collisions and cosmic rays. They used to be studied separately in the last decades but it turns out that a wise synergy pays off.

2

## 2. Total inclusive cross sections

The total cross section is an important ingredient to estimate the number of pile-up events at the LHC but also to model interactions in cosmic rays. The amount of pile-up events, occurring usually at a soft scale, increases with increasing instantaneous luminosity, and may amount to several tens for values around the nominal luminosity of  $10^{34}\text{cm}^{-2}\text{s}^{-1}$ . Total, elastic as well as inelastic cross sections can be measured using special forward proton detectors which are placed very far from the interaction point and very close to the beam since their aim is to detect a forward-going proton which scatters under a very small polar angle. The experiment dedicated for such measurements is called TOTEM and the special forward proton detector at the ATLAS side is called ALFA. They are placed more than 200 m from the interaction point and for the purpose of measuring total and elastic cross sections (which are large and dominate at low  $t$  values, where  $t$  is a four-momentum transfer squared) we use special LHC optics (characterized mainly by the betatron function,  $\beta^*$ ) and inject only a few bunches with low proton intensity. This leads to a small number of proton-proton interactions per bunch crossing (often termed “low pile-up”). The larger  $\beta^*$ , the lower  $t$  values can be reached. Figure 1 left shows

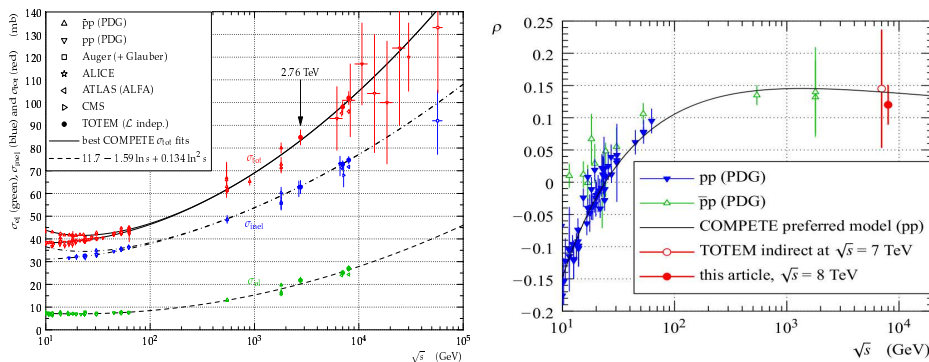


Fig. 1. Left) Compilation of the total, inelastic and elastic cross-section measurements. The continuous black lines (lower for pp, upper for  $\bar{p}p$ ) represent the best fits of the total cross-section data by the COMPETE collaboration<sup>7</sup>. The dashed line results from a fit of the elastic scattering data. The dash-dotted lines refer to the inelastic cross section and are obtained as the difference between the continuous and dashed fits. Right) The energy dependence of the  $\rho$  parameter. The hollow red circle stands for the earlier indirect determination by TOTEM<sup>8</sup>. The filled red circle represents the result from TOTEM<sup>9</sup>. The black curve gives the preferred pp model by COMPETE<sup>7</sup>, obtained without using LHC data.

a compilation of all total, inelastic and elastic cross section measurements so far together with a preliminary point from TOTEM<sup>10</sup> for the collision energy,  $\sqrt{s}$ , of 2.76 TeV. The new ATLAS results for the 8 TeV point<sup>11</sup> are also included. The inelastic cross section was recently measured by ATLAS at 13 TeV with the central detector only<sup>12</sup> and a good consistence was reached with the results based on

the special forward proton detectors as well as with predictions of PYTHIA 8<sup>13</sup>, EPOS LHC<sup>14</sup> and QGSJET-II<sup>15</sup>. An interesting feature of the elastic cross section measurement was documented by TOTEM in the 8 TeV measurement<sup>16</sup>: in the region where Coulomb interactions can be safely neglected, the exponential form of the  $t$ -slope was excluded at the level of  $7.2 \sigma$ . Similar non-exponential  $t$ -slopes were also observed at 7 and 13 TeV measurements. The explanation of this non-exponentiality is still lively discussed among theorists. If  $t$  values of the order of  $10^{-4}$  can be reached, one can then study the so called Coulomb-nuclear interference region which then enables us to measure the  $\rho$  parameter which is the ratio of real to imaginary part of the forward amplitude. Figure 1 right shows the  $\sqrt{s}$  dependence of the  $\rho$  parameter. A direct measurement of the  $\rho$  parameter by TOTEM at 8 TeV ( $\beta^* = 1$  km and  $t \sim 10^{-4}$ )<sup>9</sup> agrees within experimental uncertainties with the COMPETE fit, and another direct measurement, namely at 13 TeV and  $\beta^* = 2.5$  km, will appear soon and thus will provide a valuable level-arm for the energy dependence.

### 3. Inclusive charged particle spectra in pp

Measurements of inclusive and identified particle spectra belong to basic items in the physics programs of high-energy experiments. They are usually measured regularly at each collision energy. The multiplicity of charged particles is one of the key characteristics of high-energy hadron collisions and has been the subject of many experimental and theoretical studies because although quite simple to measure, it is quite difficult to describe it in the full measured range. Measurements of charged particle distributions probe the non-perturbative region of QCD where QCD-inspired models implemented in MC event generators are used to describe the data. Measurements are used to constrain free parameters of these models. Accurate description of low-energy strong interaction processes is essential for simulating single pp as well as multiple pp interactions in the same bunch crossing at higher instantaneous luminosities. Such pp measurements are also used as input in many models trying to describe heavy-ion results. The ALICE analysis<sup>17</sup> presents a comprehensive set of measurements of pseudorapidity density and multiplicity distributions in pp collisions over the LHC energy range from 0.9 up to 8 TeV, in 5 energy points. Three event selections are used, namely INEL which means all inelastic events, then INEL>0 which means events with at least 1 charged particle in the  $|\eta| < 1$  range, and Non-Single-Diffractive events. Figure 2 shows the multiplicity distributions at 0.9 TeV (left) and 7 TeV (middle). All models (EPOS LHC, PHOJET, PYTHIA 6 and PYTHIA 8) show big troubles in describing the whole spectrum in data but the best agreement is achieved with EPOS. Similar observations are made for the remaining  $\sqrt{s}$  points. It is also very useful to measure the energy dependence of the charged particle multiplicity at mid-rapidity, i.e. for  $|\eta| < 0.5$ , since it is related to the average energy density in the interaction of protons and it gives a reference for heavy-ion collisions. Alternatively, we can calculate

4

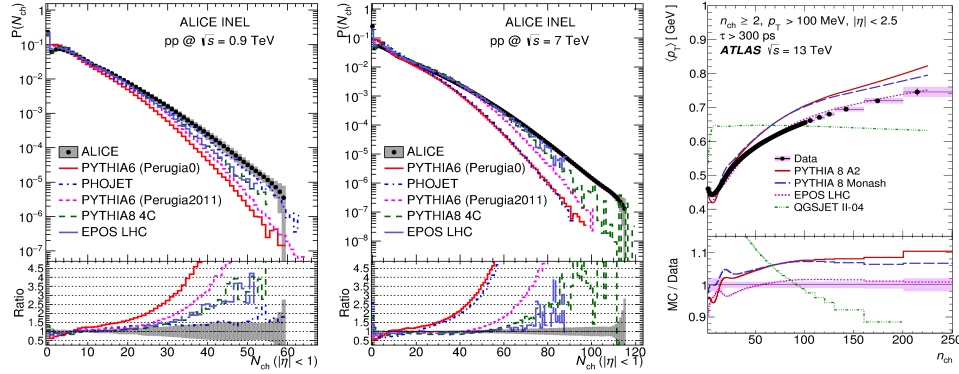


Fig. 2. Primary charged-particle multiplicities measured by: ALICE at 0.9 TeV<sup>17</sup> (left), 7 TeV<sup>17</sup> (middle) for the INEL event class in the pseudorapidity range  $|\eta| < 1.0$  and right) by ATLAS at 13 TeV<sup>18</sup> as a function of the mean  $p_T$  for events with at least two primary charged particles with  $p_T > 100$  MeV and  $|\eta| < 2.5$ , each with a lifetime  $\tau > 300$  ps. The black dots represent the data and the coloured curves the different MC model predictions. The vertical bars represent the statistical uncertainties, while the shaded areas show statistical and systematic uncertainties added in quadrature. The lower panel in each figure shows the ratio of the data to MC simulation (left and middle) or vice versa (right).

normalized  $q$ -moments ( $C_q$ ) and measure their energy dependence. KNO (Koba, Nielsen and Olesen) scaling then states that  $C_q$  stays energy-independent. Since it was reported in the past as dependent on the event selection and  $\eta$  range, ALICE came up with a comprehensive analysis covering three event classes and three  $\eta$  ranges. The conclusion of the measurement is that the KNO scaling violation increases with increasing  $\sqrt{s}$  and at a given  $\sqrt{s}$ , with increasing  $\eta$  interval.

A similar study, now at 13 TeV energy, has recently been performed and published by ATLAS<sup>18</sup>. Here only charged particles with lifetime smaller than 30 ps and larger than 300 ps are used since those with lifetime larger than 30 ps are usually strange baryons which have a low reconstruction efficiency. For comparison to previous measurements which used also these strange baryons, an extrapolation is used to include these particles. The data are compared to PYTHIA 8, EPOS LHC and QGSJET-II. PYTHIA 8 and EPOS include the effects of color coherence which is important in dense parton environments and effectively reduces the number of particles produced in MPI. PYTHIA8 splits the generation into diffractive and non-diffractive processes, the latter dominated by  $t$ -channel gluon exchange, the former is described by Pomeron-based approach. EPOS implements a parton-based Gribov-Regge theory, effective field theory describing both hard and soft scattering at the same time. QGSJET-II is based on Reggeon-field theory framework. EPOS and QGSJET-II do not rely on parton density function (PDF). Averaged  $p_T$  as a function of multiplicity increases as modeled by a colour reconnection mechanism in PYTHIA 8 and by the hydrodynamical evolution model in EPOS. QGSJET-II model which has no model for colour coherence effects describes the data poorly.

This analysis also reported that multiplicity distribution is not described perfectly by any of the models, there are large discrepancies especially at large multiplicities. Having observed similar discrepancies at all measured energies, we conclude that for every collision energy, model parameters usually need to be re-tuned in every MC generator. Unlike the multiplicity distributions, the mean particle multiplicity at mid-rapidity ( $|\eta| < 0.2$ ) measured at several  $\sqrt{s}$  points was found to be well described by PYTHIA 8 Monash and EPOS models for three event selections.

### 3.1. Forward energy flow of charged particles in $pp$

Measurements of the forward energy flow of charged and neutral particles serve to tune two types of MC models: i) those used at hadron colliders where the measurements are used to tune MPI and other soft characteristics, ii) the measurements have also an impact on the total number of muons in the extensive air showers at the ground whose measurements are still not well-described by models for cosmic rays. The CMS measurement described in<sup>19</sup> is based on using a forward calorime-

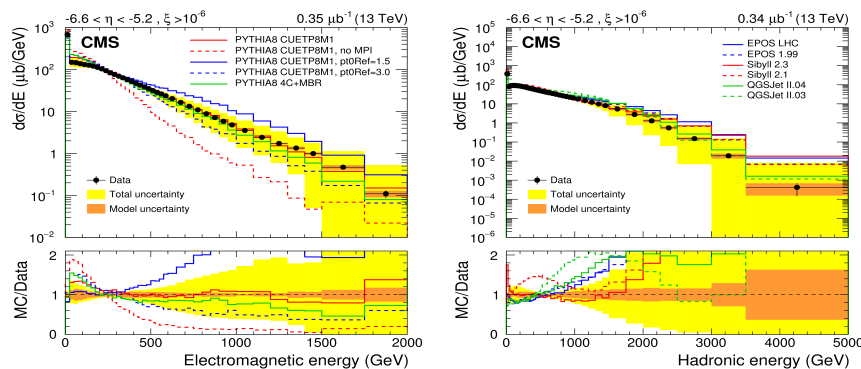


Fig. 3. Left) Differential cross section as a function of the electromagnetic energy in the region  $-6.6 < \eta < -5.2$  for events with  $\xi > 10^{-6}$  ( $\xi$  is fractional momentum loss of the incident proton). The panel shows the data compared to different PYTHIA 8 tunes. Right) Differential cross section as a function of the hadronic energy in the region  $-6.6 < \eta < -5.2$  for events with  $\xi > 10^{-6}$ . The panel shows the data compared to MC event generators mostly developed for cosmic ray induced air showers. Plots taken from Ref. 19.

ter at negative rapidities only, called CASTOR which has an electromagnetic and hadronic part, so is able to distinguish electromagnetic particles (which are mostly electrons and photons from  $\pi^0$  decays) and hadrons (mostly  $\pi^\pm$ ). The data were taken at a very low instantaneous luminosity to suppress the pile-up. In Fig. 3 left, the energy spectra of electromagnetic particles are compared to predictions of models used to describe the multihadron production at hadron colliders and from the comparisons to various MPI tunings, we conclude that the data are very sensitive to the MPI modeling. The right side of Fig. 3 documents huge deficiencies in

6

describing the spectrum of hadrons by all models used to model cosmic rays (EPOS, SYBILL and QGSJET II).

### 3.2. Forward energy flow of neutral particles in $pp$

The very forward energy flow of neutral particles is measured by a set of hodoscopes, in a dedicated experiment LHCf located at 140 m downstream of the ATLAS detector. The aim of such measurements is to improve hadronic interaction models, especially used in generators for cosmic rays. For example, modeling of  $X_{max}$  (the position of shower maximum) needs the total cross section for the collision of proton with air, but also the spectra of identified particles going very forward. And modeling of the hadronic interactions in those generators is based on correlations between spectra of particles going central versus those going forward. This is perfectly possible since LHCf uses the same interaction point as the ATLAS detector which measures very precisely the central production. A first common analysis of the same event sample analyzed by ATLAS and LHCf is in preparation. Figure 4

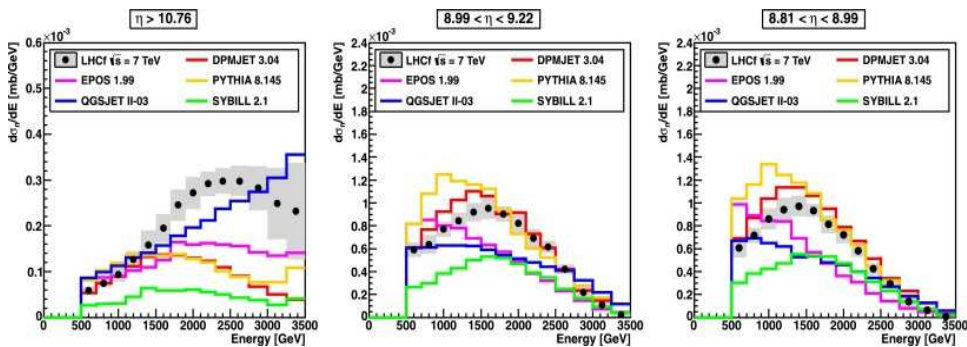


Fig. 4. A comparison of the LHCf neutron energy spectra measured in 7 TeV  $pp$  collisions<sup>20</sup> with model predictions. The black markers and gray shaded areas show the corrected data and the systematic uncertainties, respectively.

shows the energy spectra of neutrons from the 7 TeV  $pp$  collisions<sup>20</sup> where large deficiencies in all models used for modeling cosmic rays (EPOS, QGSJET, DPMJET<sup>21</sup> and SIBYLL<sup>22</sup> and also PYTHIA 8) are observed. The  $p_T$  spectra of  $\pi^0$  produced in 7 TeV  $pp$  collisions<sup>23</sup> in a fine  $\eta$  binning are quite well described by EPOS, less well described by DPMJET. Recently, photon energy spectra have been measured in 13 TeV  $pp$  collisions<sup>24</sup> and again all models are observed to have difficulties in describing the whole measured spectrum.

### 4. Identified particle spectra in $pp$ , $pPb$ and $PbPb$

In order to identify particle species, each experiment has sophisticated identification procedures usually based on the ionization energy loss,  $dE/dx$ , or other techniques.

In the ALICE analysis<sup>25</sup>, strange hadrons with different strangeness content are identified and a ratio of multiplicity of strange hadrons to pions is plotted in Fig. 5 left as a function of multiplicity density in the center of the detector for all three collision systems: going from relatively low multiplicity densities occurring in  $pp$  collisions over middle densities seen in  $pPb$  collisions up to large densities corresponding to  $PbPb$  collisions. We observe that the integrated yields of strange and multi-strange particles relative to pions, increase significantly with the charged particle multiplicity and that the yield ratios measured in  $pp$  collisions agree with  $pPb$  measurements at similar multiplicities. This is a first observation of a strangeness

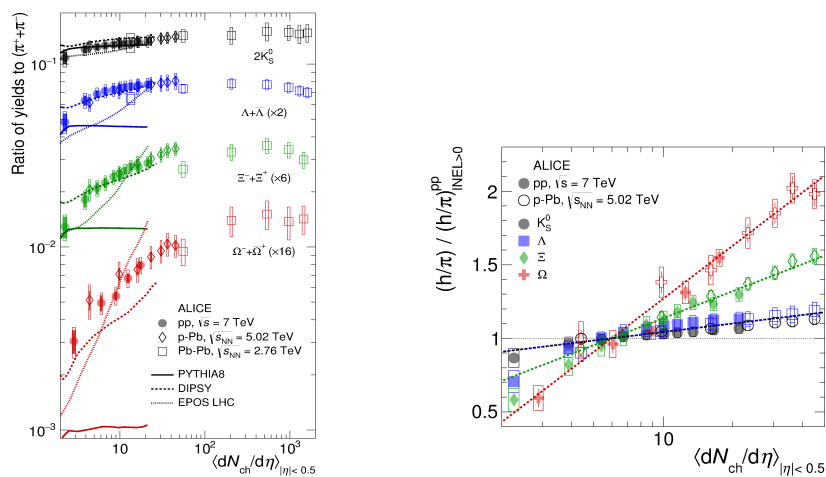


Fig. 5. Left) The  $p_T$  integrated yield ratios to pions as a function of  $\langle dn_{ch}/d\eta \rangle$  measured in  $|\eta| < 0.5$ . The error bars show the statistical uncertainty, whereas the empty and dark-shaded boxes show the total systematic uncertainty and the contribution uncorrelated across multiplicity bins, respectively. The values are compared to calculations from MC models<sup>13,14,27</sup> and to previous results obtained by ALICE in  $pPb$  and  $PbPb$  collisions. Right) Particle yield ratios to pions normalized to the values measured in the inclusive  $pp$  sample. The error bars show the statistical uncertainty. The common systematic uncertainties cancel in the double-ratio. The empty boxes represent the remaining uncorrelated uncertainties. The lines represent a simultaneous fit of the results with an empirical scaling formula. Plots taken from Ref. 25.

enhancement in high-multiplicity  $pp$  collisions. In very high-multiplicity  $pPb$  collisions, the strangeness production reaches values similar to those observed in  $PbPb$  collisions, where a quark-gluon plasma (QGP) is formed. QGP is matter in a phase of deconfined quarks and gluons which is created at sufficiently high temperatures and energy densities which is usually reached in collisions of heavy ions with high energies. Strangeness enhancement has been proposed as one of the main signatures of formation of QGP<sup>26</sup>. We see that none of the three models is able to describe the data but DIPSY<sup>27</sup>, a special model using color ropes, describes data best. In the analysis<sup>25</sup>, the ratio of baryon to meson yields is also studied and it is observed that none of the models is able to describe the data. In Fig. 5 right, the

strangeness enhancement with respect to inclusive samples is plotted: here we see a clear strangeness hierarchy, namely the slope increasing with increasing strangeness content, and in addition, the same hierarchy as measured already for  $pPb$  data is observed. We conclude that mass and multiplicity dependencies of the strangeness enhancement as well as of the spectral shapes (not shown here, see<sup>25</sup>) remind the patterns seen for  $pPb$  and  $PbPb$  collisions which can be understood assuming a collective expansion of the system in the final state.

Absolute yields and  $p_T$  spectra of identified particles in hadron-hadron collision are usually used to improve the modeling of various key ingredients of MC event generators, such as MPI, parton hadronization, and final state effects such as parton correlations in color,  $p_T$ , spin, baryon and strangeness number, and collective flow. Parton hadronization and final state effects are mostly constrained from  $e^+e^-$  data whose final states are dominated by simple  $q\bar{q}$  states, whereas low  $p_T$  hadrons at LHC come from fragmentation of multiple gluons, so called minijets. This is also the reason why the production of baryons and strange hadrons in  $pp$  collisions is not well reproduced by current generators, and hence makes a good motivation for this study. In addition, identified particle spectra serve as an important reference for high-energy HI studies. This CMS study<sup>28</sup> used data with negligible pile-up. Pions, kaons and protons are identified using  $dE/dx$ , a specific ionization which works very well for momenta lower than 1.2, 1.1 and 1.7 GeV for pions, kaons and protons, respectively. All particle species are limited to the region  $|\eta| < 1.0$ . And because transverse momenta as low as 0.1 GeV are measured, special tracking algorithms were used with high reconstruction efficiency and low background. These algorithms feature special track seeding and cleaning, hit cluster shape filtering, modified trajectory propagation and track quality requirements. Figure 6

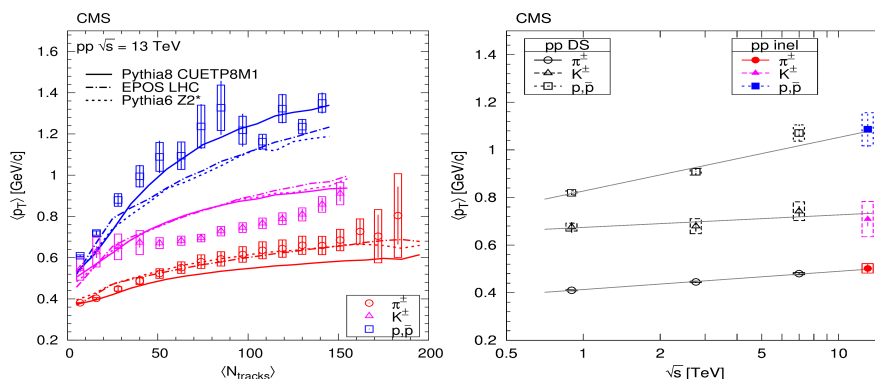


Fig. 6. Average  $p_T$  of charged-averaged pions, kaons and protons in the range  $|\eta| < 1$  as functions: left) of the corrected track multiplicity for  $|\eta| < 2.4$ , computed assuming a Tsallis-Pareto distribution in the unmeasured range. Curves indicate predictions from PYTHIA 8, EPOS and PYTHIA 6; right) of  $\sqrt{s}$ . The curves show linear fit in  $\ln s$ . Error bars indicate the uncorrelated combined uncertainties, while boxes show the uncorrelated systematic uncertainties. Plots taken from Ref. 28.



left shows the average  $p_T$  as a function of multiplicity in the event. We can notice that for kaons, all models overshoot the data. While the low multiplicity region is well modeled by the generators, the high multiplicity region needs some tuning of baryon and/or strangeness production. Figure 6 right shows a rising evolution of the average  $p_T$  with  $\sqrt{s}$ . This collision energy evolution of the average  $p_T$  provides useful information on the so called saturation scale of the gluons in proton.

### 5. Underlying event in $pp$

The hard scattering is accompanied by interactions of a soft nature, namely those coming from the rest of the proton-proton collision. They can come from the initial state radiation (ISR), final state radiation (FSR), MPI and from color reconnections (CR, namely from the QCD evolution of colour reconnections between the hard scatter and beam remnants). A combination of contributions from all these processes is called underlying event (UE) which is important to consider and measure (or estimate) since:

- These processes can not be completely described by perturbative QCD, and require phenomenological models, whose parameters are tuned by means of fits to data.
- Final state (or its part) coming from UE can mimic a signal final state, for example the same-sign WW production from MPI can mimic final state of the same-sign dilepton SUSY searches.
- It can affect isolation criteria applied to photons and charged leptons.
- It can affect the vertex reconstruction efficiency. For example the primary vertex in the process  $H \rightarrow \gamma\gamma$  can be partly determined from the charged particles originating from UE.

An usual procedure of estimating the amount of UE is spatially dividing tracks in each event according to their azimuthal angle to the Towards region (where the highest  $p_T$  jet points), the Away region (where the second highest  $p_T$  jet points) and then we have two Transverse regions where one of them contains imprints of ISR and FSR and the other one has the least activity (so called Transverse-min) — this one is believed to be the most sensitive to UE. The usual observables are average track multiplicity per unit area and average scalar sum of track  $p_T$  per unit area.

Figures 7 left and middle concentrate on the UE-dominated region studied in ATLAS events containing at least one charged particle with  $p_T > 1$  GeV<sup>29</sup>. The left plot shows the multiplicity evolution of the average  $p_T$ , it can also be seen as a correlation between two “soft” properties. It shows a balance between  $p_T$  sum and multiplicity. This balance is affected in some models by CR which typically increases the  $p_T$  per particle. The description by all models is within 5%. EPOS gives in general best description at low  $p_T$  of the leading particle, but is the worst when the  $p_T$  of the leading particle is above 10 GeV (not shown here). The middle

plot shows the evolution of the  $p_T$  sum density with  $p_T$  of the leading particle, for three collision energies. The initial rapid rise up to  $p_T^{\text{lead}} \approx 5$  GeV after which the density stabilizes around one charged particle or 1 GeV per unit  $\phi - \eta$  area is known as the “pedestal effect”. It reflects a reduction of the  $pp$  impact parameter with increasing  $p_T^{\text{lead}}$  and hence the transition between the minimum bias and hard scattering regimes. The right plot shows a similar trend, namely the evolution of

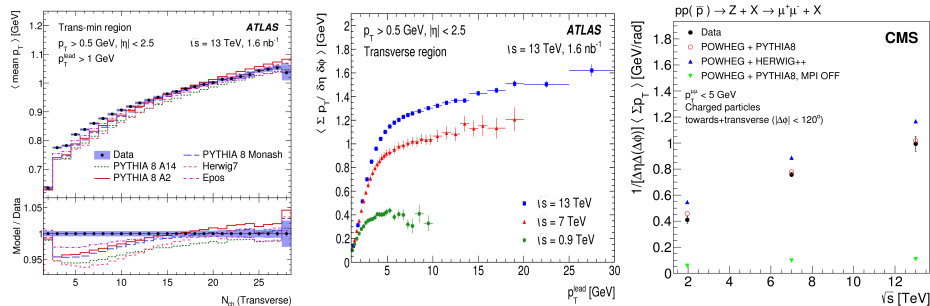


Fig. 7. Left) Mean charged-particle average  $p_T$  as a function of charged-particle multiplicity in the transverse-min azimuthal region<sup>29</sup>. The error bars on data points represent statistical uncertainty and the blue band the total combined statistical and systematic uncertainty. Middle) Mean sum  $p_T$  densities as a function of transverse momentum of the leading charged particle measured for  $\sqrt{s} = 0.9, 7$  TeV<sup>30</sup> and 13 TeV<sup>29</sup>. Right) Sum  $p_T$  density, with  $p_{\mu\mu} < 5$  GeV as a function of  $\sqrt{s}$  for data<sup>31</sup> and predictions from simulations by POWHEG+PYTHIA 8 and POWHEG+HERWIG++. The predictions of POWHEG+PYTHIA 8 without MPI are also shown. Error bars represent the statistical and systematic uncertainties added in quadrature.

$p_T$  average per event with increasing collision energy. It is a CMS<sup>31</sup> analysis based on Drell-Yan events selected using a detection of a dimuon pair. From a comparison to various models and mainly to PYTHIA with and without MPI, we can clearly see the importance of MPI in modeling the UE activity.

## 6. 2-particle azimuthal correlations in $pp$ , $pPb$ and $PbPb$

Soft processes are also in the heart of heavy-ion collisions<sup>32</sup>. In the HI collisions at LHC, it is believed that quark-gluon plasma is created. The conditions for the phase transition are created, the system gets close to the thermal equilibrium and expands collectively. The expansion means that the matter cools down and hadrons are formed. The aim is to measure macroscopic properties of the QGP and study its microscopic laws. Usually  $PbPb$  collisions serve to create and study QGP, the  $pPb$  collisions serve as a sort of control experiment (cold nuclear matter effects (e.g. modifications to PDF)) and the  $pp$  collisions serve as reference data. But recently, striking similarities were observed between these three collision systems. Phenomena considered fundamental for QGP are now seen also in  $pPb$  and even  $pp$ . These were discovered in high-multiplicity events but they may be relevant also

for minimum bias events which would, in turn, have important consequences for all hadronic collisions. We speak especially about the ridge observation. The ridge was first observed in central HI collisions as 2-particle long-range correlations ( $\Delta\eta > 2$ ) on a near side ( $\Delta\phi \approx 0$ ) and it is believed to be a result of collective hydrodynamic expansion of hot and dense nuclear matter created in the overlap region. The 2-particle correlations exhibit also the so-called away-side peak coming from the other lower-energy jet. The ridge is usually described by Fourier decomposition using a term  $\cos(n\Delta\phi)v_n$  where  $v_n$  is a single-particle anisotropy harmonics. Unexpectedly ridge structures were also measured in  $pPb$  and even in  $pp$  at high multiplicities. Currently the origin of the ridges in these small collision systems is lively debated. Is it hydrodynamics like in QGP which would mean a final state effect? Or is it due to initial state fluctuations (as embedded in Color Glass Condensate (CGC) model<sup>33</sup> using gluon saturation)? Or perhaps these long range correlations come from hadronization described by ropes<sup>27</sup>? Or from collisions of thin flux tubes<sup>34</sup>? Definitely the ridge is a testing ground to study complementarity between dynamical and hydrodynamical models.

Particle correlations are a very powerful tool to study properties of multihadron production in general. Several production mechanisms can be studied simultaneously. The baseline mechanism underlying all correlations is a global conservation of momentum and energy as well strangeness, baryon number and electric charge. Other phenomena, including mini-jets, elliptic flow, Bose-Einstein correlations (BEC) and resonance decays are source of additional correlations and all those sum up.

By studying the  $\Delta\phi$  projections of 2-particle correlations around the near-side and away-side peak, it was observed e.g. by LHCb<sup>35</sup> using 5.02 TeV  $pPb$  data and by ALICE<sup>36</sup> using 2.76 TeV  $PbPb$  data that both peaks increase with multiplicity and that the size of the near-side peak is maximal for particle with  $1 < p_T < 2$  GeV. To study the long-range correlations, however, we have to subtract 2-particle correlations coming from the so called “non-flow” which includes resonance decays and dijets. There are several methods to do that, one class of methods tries to subtract the non-flow using low-multiplicity events. It also turns out that the extraction of collective flow in  $pp$  collisions strongly depends on the event selection and also on the purity of the non-flow extraction as documented e.g. in the analysis<sup>37</sup>.

Figure 8 left shows an almost linear increase of 2-particle correlations with event multiplicity for all three collision systems measured by CMS<sup>38</sup>. The size of these correlations is biggest for HI collisions, while it is smallest for  $pp$  collisions. Figure 8 right then shows a measurement by ATLAS<sup>39</sup> of the  $v_2$  quantity, the elliptic flow harmonics, again for all three collision systems now as a function of multiplicity. The measurement shows that  $v_2$  from  $pPb$  is smaller than that extracted from the  $PbPb$  collisions but originally much smaller values from  $pPb$  collisions were expected reflecting the big difference in sizes of the  $PbPb$  and  $pPb$  systems.

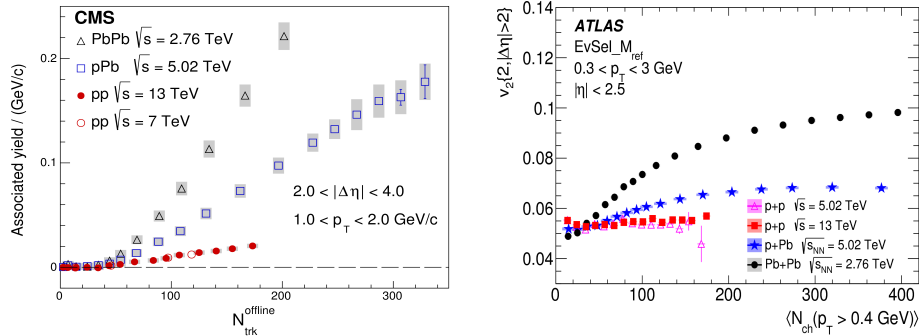


Fig. 8. Left) Associated yield of long-range near-side two-particle correlations for  $1 < p_T < 2$  GeV in  $pp$  collisions at  $\sqrt{s} = 13$  and 7 TeV,  $pPb$  collisions at  $\sqrt{s} = 5.02$  TeV, and  $PbPb$  collisions at  $\sqrt{s} = 2.76$  TeV. The error bars correspond to the statistical uncertainties, while the shaded areas denote the systematic uncertainties. Plot taken from Ref. 38. Right) Comparison of  $v_2\{2, |\Delta\eta| > 2\}$  as a function of  $\langle N_{\text{ch}} \rangle (p_T > 0.4 \text{ GeV})$  for  $pp$  collisions at  $\sqrt{s} = 5.02$  and 13 TeV,  $p+Pb$  collisions at  $\sqrt{s} = 5.02$  TeV and low-multiplicity  $Pb+Pb$  collisions at  $\sqrt{s} = 2.76$  TeV, and for reference particles with  $0.3 < p_T < 3$  GeV. The error bars and shaded boxes denote statistical and systematic uncertainties, respectively. Plot taken from Ref. 39.

## 7. Multi-particle azimuthal correlations in $pp$ , $pPb$ and $PbPb$

In the light of difficulties with the residual non-flow which the 2-particle correlations suffer from, methods based on multi-particle correlations started to be more widely used. It was proved that multi-particle correlations are more robust with respect to the non-flow but it is clear that they are also more statistically demanding. The method often used is to build cumulants  $c_n\{2k\}$  (of the  $n$ -th order based on  $2k$ -particle correlations) and calculate flow harmonics  $v_n\{2k\}$  from them. A novel method, the three-subevent method, has recently been proposed by ATLAS<sup>37</sup> which turns out to be quite effective in reducing the non-flow and moreover it provides negative values of cumulants  $c_2\{4\}$ ,  $c_2$  calculated from 4-particle correlations, which is required to get positive  $v_2\{4\}$ . Figure 9 from the multi-particle correlation study by CMS<sup>40</sup> shows  $v_2$  coefficients calculated using 2-, 3-, 4-, 6- and even 8-particle correlations as functions of multiplicity for all three collision systems. First the results say that  $v_2$  from 4-particle correlations are smaller than  $v_2$  from 2-particle correlations in  $pPb$  and  $PbPb$  collisions - that was expected for long-range correlations. We however observe smaller  $v_2\{4\}$  than  $v_2\{2\}$  values for the  $pp$  system (even larger differences are reported using the three-subevent method in the analysis<sup>37</sup>) and a similarity between  $v_2\{4\}$  and  $v_2\{6\}$  values in all three collision systems. All these findings suggest again that some collective effects are occurring even in  $pp$  collisions.

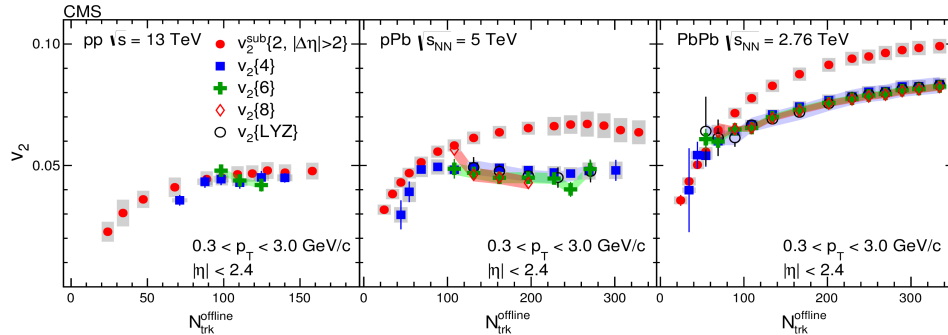


Fig. 9. Left) The  $v_2$  values calculated from 2-, 4-, 6- and 8-particle correlations as functions of multiplicity of charged particles, averaged over  $0.3 < p_T < 3.0$  GeV and  $|\eta| < 2.4$ , in  $pp$  collisions at  $\sqrt{s} = 13$  TeV (left), in  $pPb$  collisions at  $\sqrt{s} = 5.02$  TeV<sup>41</sup> (middle) and in  $PbPb$  collisions at  $\sqrt{s} = 2.76$  TeV<sup>41</sup> (right). The error bars correspond to the statistical uncertainties, while the shaded areas denote the systematic uncertainties. Plot taken from Ref. 40.

## 8. Angular correlations of identified particles in $pp$

The 2-particle correlations can also be studied with identified particles. By choosing specific particle types, we select a specific combination of quantum numbers (strangeness, baryon number) that may manifest in the measured correlations. The correlations should also be sensitive to the details of particle production, including the parton fragmentation. In this ALICE study<sup>42</sup> the near-side peak structure is studied. It is a combination of at least three effects: i) fragmentation of hard-scattered partons, ii) resonance decays and iii) femtoscopic correlations (BEC for identical bosons, Fermi-Dirac anticorrelations for identical fermions, Coulomb and strong final-state interactions). For pairs of same mesons, the near-side peak comes from the minijet mechanism and BEC. The correlations of particle-antiparticle pairs also include a minijet like structure on the near-side as well as on the away-side. For pairs of non-identical particles Bose-Einstein and Fermi-Dirac effects are not present, however, resonances play a significant role. In contrast to same-sign meson correlations, the baryon-baryon (or antibaryon-antibaryon) distributions for identical proton and lambda baryon pairs show a qualitatively different effect, namely a near-side depression instead of the peak. The correlations for same-sign pions and kaons as well as same-sign protons and  $\Lambda$  baryons are shown in Fig. 10, projected onto the  $\Delta\phi$  axis and compared with several MC generators. While for mesons (a-b), the description of the apparent near-side and small away side peaks is reasonable, all event generators fail by giving positive correlations for protons and  $\Lambda$  baryons (c-d), where data show a significant depression. It should be noted that these generators conserve the local baryon number and do not include quantum statistical effects such as Fermi-Dirac anticorrelations. Several sources of this depression were studied in this analysis and it was shown that neither Fermi-Dirac anticorrelations nor strong final state effects nor local baryon number conservation

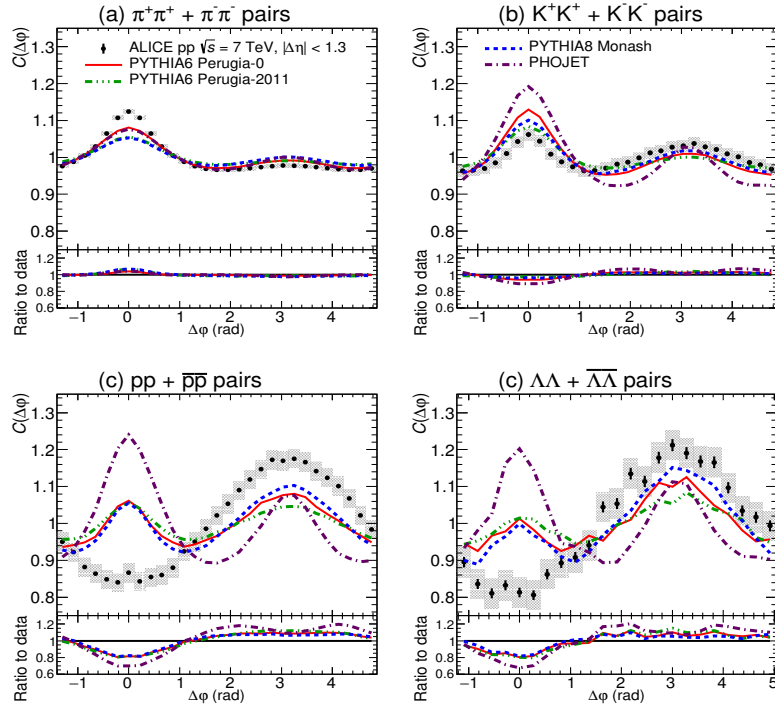


Fig. 10. The  $\Delta\eta$  integrated projections of correlation functions for combined pairs of (a)  $\pi^+\pi^+ + \pi^-\pi^-$ , (b)  $K^+K^+ + K^-K^-$ , (c)  $pp + \bar{p}\bar{p}$  and (d)  $\Lambda\Lambda + \bar{\Lambda}\bar{\Lambda}$ , obtained from ALICE data and four Monte Carlo models (PYTHIA 6 Perugia-0, PYTHIA 6 Perugia-2011, PYTHIA 8 Monash, PHOJET). Bottom panels show ratios of MC models to ALICE data. Statistical (bars) and systematic (boxes) uncertainties are plotted. Plot taken from Ref. 42.

can explain this depression. So we conclude that something essential is missing in the string fragmentation.

### 9. Bose-Einstein correlations in $pp$ , $pPb$ and $PbPb$

ATLAS has recently published a BEC study with 7 TeV data based on particles with  $p_T$  as low as 100 MeV<sup>43</sup>. BE correlations are defined using  $c_2$ , the 2-particle cumulants for identical particles, and are usually plotted as a ratio of same-sign to opposite-sign  $c_2$  cumulants as a function of  $Q$  which is the momentum difference of the particles in a pair. This  $c_2(Q)$  dependence is then fitted using the function  $C_2 = [1 + \Omega(\lambda, R)](1 + \epsilon Q)$  where  $\lambda$  represents a correlation strength and  $R$  represents a size of the correlation source. The size of the source has been measured as a function of event multiplicity and particle  $p_T$ . The multiplicity dependence represented in Fig. 11 left shows an interesting feature, namely a rise and then a sudden stop and a saturation from multiplicities of about 50. This saturation at high multiplicities is seen for the first time at all. The  $p_T$  dependence of  $R$  was measured to decrease

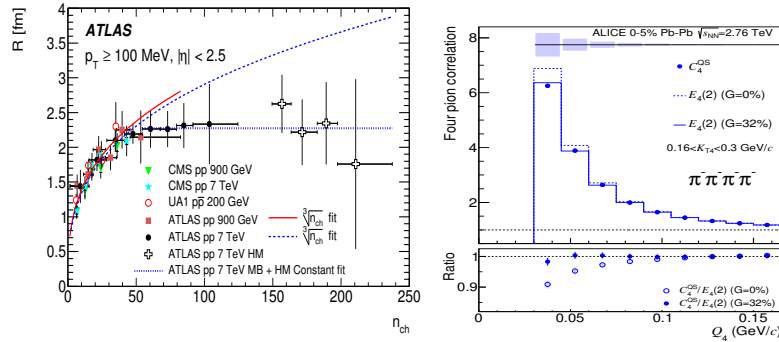


Fig. 11. Left) Multiplicity  $n_{ch}$  dependence of the parameter  $R$  obtained from the exponential fit to the two-particle double-ratio correlation functions  $R_2(Q)$  at  $\sqrt{s} = 0.9$  and 7 TeV, compared to the equivalent measurements of the CMS<sup>44</sup> and UA1<sup>45</sup> experiments. The solid and dashed curves are the results of the  $\sqrt[3]{n_{ch}}$  for  $n_{ch} < 55$  fits. The dotted line is a result of a constant fit to minimum-bias and high-multiplicity events data at 7 TeV for  $n_{ch} \geq 55$ . The error bars represent the quadratic sum of the statistical and systematic uncertainties. Plot taken from Ref. 43. Right) Same-charge four-pion full correlations versus  $Q_4$  (see the text). Measured (points) and expected (histograms) correlations of the first type are shown. Dashed and solid block histograms show the expected correlations based on  $G=0$  and  $G=32\%$  fraction of coherent correlations, respectively. Systematic uncertainties are shown at the top. The bottom panel shows the ratio of measured to the expected correlations. The systematic uncertainties on the ratio are shown with a shaded blue band ( $G=0$ ) and with a thick blue line ( $G=32\%$ ). Plot taken from Ref. 48.

for all multiplicity classes. A similar tendency was measured in another ATLAS analysis of  $pPb$  data<sup>46</sup>. Also in the LHCb study<sup>47</sup>,  $R$  was measured to increase with multiplicity, while  $\lambda$  to decrease with multiplicity, so in accordance with observations made by the other LHC experiments, we can conclude that larger sources are more coherent.

Multi-pion BE correlations have also been measured in all three collision systems by ALICE<sup>48</sup>. In Fig. 11 right we can see the 4-pion correlations as a function of  $Q$  between these pions and the ratio of these measured 4-particle correlations to the expected ones from 2-pion correlations. While for  $pp$  and  $pPb$  collisions, no suppression is seen, in  $PbPb$ , a clear suppression of both the 4-pion and 3-pion (not shown here) correlations is observed. Interestingly, if a 32%-fraction of coherent correlations is assumed, the suppression is explained for the 4-pion correlation, while it does not help to the 3-pion correlations.

## 10. Hadronic chains

The origin of the enhanced production of pairs of identical particles is usually studied using BEC, believed to come from an incoherent particle production (see the previous section). An alternative approach to BEC is a causality-respecting model of quantized fragmentation of a 3D QCD string as a consequence of coherent hadron emission. This approach is based on studying hadronic chains<sup>49</sup> using helical

strings<sup>50</sup> and utilized in a recent ATLAS analysis<sup>51</sup>. It studies hadronization effects using the same ATLAS data as in the BEC study<sup>43</sup>, namely again same-sign and opposite-sign identical particle pairs. In the Lund hadronization, used in PYTHIA, there is a randomly broken 1D string and no cross-talk between break-up vertices. In the model of quantized helical (3D) string, one tries to make use of causality (in other words the cross-talk between break-up vertices) which gives two parameters:  $\kappa R$  and  $\Delta\phi$ . This model predicts that the hadron spectra follow a simple quantized pattern:  $m_T = n\kappa R\Delta\phi$ , so that  $\kappa R$  and  $\Delta\phi$  can be fixed using known masses of pseudoscalar mesons. Then one can predict momentum difference  $Q$  for pairs of ground-state hadrons for various pair rank differences,  $r$ . Adjacent (opposite-sign) pions are then predicted to be produced with  $p_T$  difference of 266 MeV, while the like-sign pion pairs with rank difference 2 should have 91 MeV. Figure 12 left rep-

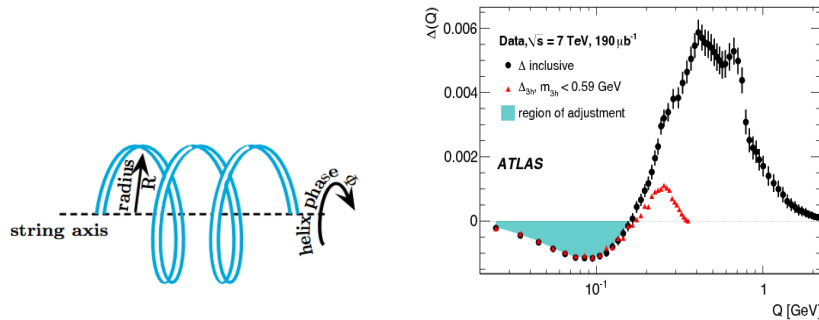


Fig. 12. Left) Parameterization of the helical shape of the QCD string. Right) The corrected  $\Delta(Q)$  is compared with the corrected contribution from low-mass three-hadron chains  $\Delta_{3h}(Q)$ . The chain mass limit is set to a value of  $m_{3h}^{cut} = 0.59$  GeV, which reproduces the excess in the inclusive like-sign pair production at low  $Q$  (shaded area). Bin errors indicate the combined statistical and reconstruction uncertainty. Plots taken from Ref. 51.

resents a parameterization of the helical shape of the QCD string, while the plot on right showing a ratio of differences between number of opposite-sign and same-sign charged particles to the number of charged particles,  $[N(OS)-N(SS)]/N_{ch}$ , plotted as a function of  $Q$ , documents that the low- $Q$  region is described by this new model of fragmentation using helical strings. The very low- $Q$  region is predicted to be populated exclusively by the same-sign pairs (which means the rank  $r = 2$ ). The further study then showed that the source of these correlations are 3-hadron chains.

## 11. Summary

This text summarizes recent soft QCD measurements from six LHC experiments and attempts to document the importance of soft QCD physics in a number of aspects. For example, the soft QCD results serve as input for modeling pile-up at



LHC and interactions in cosmic rays. They also greatly help in a better understanding of the hadronization mechanism, typically a mixture of processes dominating at low transverse momenta. Work on improving hadronization models is currently ongoing and involves a better treatment of color-confining objects such as strings and ropes. It is also evident that the effect of underlying event is non-negligible at LHC energies. Finally it was indicated that by studying particle correlations, we gain not only a powerful tool to learn more about multihadron production, but to investigate striking similarities between three collision systems at LHC, namely  $PbPb$ ,  $pPb$  and  $pp$ . With a limited set of analyses we demonstrated that all collision systems are useful for soft QCD studies, nicely complementing each other. Let us also note that the performant LHC machine and experiments unprecedentedly provide high-statistics and at the same time high-precision data samples which enable us to estimate reliably many sources of systematic uncertainties. Sophisticated techniques are used to measure very low  $p_T$  particles, to efficiently subtract many sources of background and to make use of unfolding techniques in several dimensions. This way, the precision data help to understand unexplained phenomena and to develop or to reject various theoretical models. We reported about similar phenomena observed in  $PbPb$ ,  $pPb$  and  $pp$  (high multiplicity) collisions, namely about strangeness enhancement and collectivity effects. The primordial question currently discussed in the HI community is why these effects are observed in small systems such as  $pPb$  and  $pp$ . We also conclude that the near-side ridge may be a good testing ground to study complementarity between hydrodynamics/QGP and dynamics models (CGC/saturation/ropes).

## 12. Acknowledgement

Supported by the project LG15052 of the Ministry of Education, Youth and Sports of the Czech Republic. Author wishes to thank Edward Sarkisyan-Grinbaum for helpful discussions.

## References

1. ALICE Collab., *The ALICE experiment at the CERN LHC*, *JINST* **3**, S08002 (2008).
2. ATLAS Collab., *The ATLAS Experiment at the CERN Large Hadron Collider*, *JINST* **3**, S08003 (2008).
3. CMS Collab., *The CMS Experiment at the CERN LHC*, *JINST* **3**, S08004 (2008).
4. LHCb Collab., *The LHCb Detector at the LHC*, *JINST* **3**, S08005 (2008).
5. LHCf Collab., *The LHCf detector at the CERN Large Hadron Collider*, *JINST* **3**, S08006 (2008).
6. TOTEM Collab., *The TOTEM experiment at the CERN Large Hadron Collider*, *JINST* **3**, S08007 (2008).
7. COMPETE Collab., *Benchmarks for the forward observables at RHIC, the Tevatron Run II and the LHC*, *Phys. Rev. Lett.* **89**, 201801 (2002).
8. TOTEM Collab., *Luminosity-independent measurements of total, elastic and inelastic cross-sections at  $\sqrt{s} = 7$  TeV*, *Europhys. Lett.* **101**, 21004 (2013).

9. TOTEM Collab., *Measurement of Elastic pp Scattering at  $\sqrt{s} = 8$  TeV in the Coulomb-Nuclear Interference Region - Determination of the  $\rho$  Parameter and the Total Cross-Section*, *Eur. Phys. J. C* **76**, 661 (2016).
10. M. Deile for the TOTEM Collab., talk at the conference EDS Blois 2017, Prague, Czech Rep.
11. ATLAS Collab., *Measurement of the total cross section from elastic scattering in pp collisions at  $\sqrt{s} = 8$  TeV with the ATLAS detector*, *Phys. Lett. B* **761**, 158 (2016).
12. ATLAS Collab., *Measurement of the Inelastic Proton-Proton Cross Section at  $\sqrt{s} = 13$  TeV with the ATLAS Detector at the LHC*, *Phys. Rev. Lett.* **117**, no.18, 182002 (2016).
13. T. Sjöstrand, S. Mrenna, and P. Z. Skands, *A Brief Introduction to PYTHIA 8.1*, *Comput. Phys. Commun.* **178**, 852 (2008).
14. T. Pierog *et al.*, *EPOS LHC: Test of collective hadronization with data measured at the CERN Large Hadron Collider*, *Phys. Rev. C* **92** no. 3, 034906 (2015).
15. S. Ostapchenko, *Monte Carlo treatment of hadronic interactions in enhanced Pomeron scheme: I. QGSJET-II model*, *Phys. Rev. D* **83**, 014018 (2011).
16. TOTEM Collab., *Evidence for Non-Exponential Elastic Proton-Proton Differential Cross-Section at Low  $|t|$  and  $\sqrt{s} = 8$  TeV by TOTEM*, *Nucl. Phys. B* **899**, 527 (2015).
17. ALICE Collab., *Charged-particle multiplicities in proton-proton collisions at  $\sqrt{s} = 0.9$  to 8 TeV*, *Eur. Phys. J. C* **77**, 33 (2017).
18. ATLAS Collab., *Charged-particle distributions at low transverse momentum in  $\sqrt{s} = 13$  TeV pp interactions measured with the ATLAS detector at the LHC* *Eur. Phys. J. C* **76**, 502 (2016).
19. CMS Collab., *Measurement of the inclusive energy spectrum in the very forward direction in proton-proton collisions at  $\sqrt{s} = 13$  TeV*, *J. High En. Phys.* **08**, 046 (2017).
20. LHCf Collab., *Measurement of very forward neutron energy spectra for 7 TeV proton-proton collisions at the Large Hadron Collider*, *Phys. Lett. B* **750**, 360 (2015).
21. F. W. Bopp *et al.*, *Antiparticle to Particle Production Ratios in Hadron-Hadron and d-Au Collisions in the DPMJET-III Monte Carlo*, *Phys. Rev. C* **77**, 014904 (2008).
22. E.-J. Ahn *et al.*, *Cosmic ray interaction event generator SIBYLL 2.1*, *Phys. Rev. D* **80**, 094003 (2009).
23. LHCf Collab., *Measurements of longitudinal and transverse momentum distributions for neutral pions in the forward-rapidity region with the LHCf detector*, *Phys. Rev. D* **94**, 032007 (2016).
24. LHCf Collab., *Measurement of forward photon-energy spectra for  $\sqrt{s} = 13$  TeV proton-proton collisions with the LHCf detector*, CERN-EP-2017-051, *arXiv:1703.07678 [hep-ex]*.
25. ALICE Collab., *Enhanced production of multi-strange hadrons in high-multiplicity proton-proton collisions*, *Nat. Phys.* **13**, 535 (2017).
26. P. Koch, B. Muller and J. Rafelski, *Strangeness in Relativistic Heavy Ion Collisions*, *Phys. Rept.* **142**, 167 (1986).
27. C. Bierlich and J. R. Christiansen, *Effects of Colour Reconnection on Hadron Flavour Observables*, *Phys. Rev. D* **92**, 094010 (2015).
28. CMS Collab., *Measurement of charged pion, kaon, and proton production in proton-proton collisions at  $\sqrt{s} = 13$  TeV*, CERN-EP-2017-091, *arXiv:1706.10194 [hep-ex]*.
29. ATLAS Collab., *Measurement of charged-particle distributions sensitive to the underlying event in  $\sqrt{s} = 13$  TeV proton-proton collisions with the ATLAS detector at the LHC*, *J. HEP* **03**, 157 (2017).

30. ATLAS collab., *Measurement of underlying event characteristics using charged particles in pp collisions at  $\sqrt{s} = 900$  GeV and 7 TeV with the ATLAS detector*, *Phys.Rev. D* **83**, 112001 (2011).
31. CMS Collab., *Measurement of the underlying event using the Drell-Yan process in proton-proton collisions at  $\sqrt{s} = 13$  TeV*, CERN-EP-2017-249, arXiv:1711.04299 [hep-ex].
32. M. Sumbera and R. Pasechnik, *Phenomenological Review on QuarkGluon Plasma: Concepts vs. Observations*, *Universe* **3**, no.1, 7 (2017).
33. L.D. McLerran and R. Venugopalan, *Computing quark and gluon distribution functions for very large nuclei*, *Phys. Rev. D* **49**, 2233 (1994).
34. J. D. Bjorken et al., *Possible multiparticle ridge-like correlations in very high multiplicity proton-proton collisions*, *Phys. Lett. B* **726**, 344 (2013).
35. LHCb Collab., *Measurements of long-range near-side angular correlations in  $\sqrt{s} = 5.02$  TeV proton-lead collisions in the forward region*, *Phys. Lett. B* **762**, 473 (2016).
36. ALICE Collab., *Evolution of the longitudinal and azimuthal structure of the near-side jet peak in Pb-Pb collisions at  $\sqrt{s} = 2.76$  TeV*, *Phys. Rev. C* **96**, no.3, 034904 (2017).
37. ATLAS Collab., *Measurement of multi-particle azimuthal correlations with the subevent cumulant method in pp and p+Pb collisions with the ATLAS detector at the LHC*, CERN-EP-2017-160, arXiv:1708.03559 [hep-ex].
38. CMS Collab., *Measurement of Long-Range Near-Side Two-Particle Angular Correlations in pp Collisions at  $\sqrt{s} = 13$  TeV*, *Phys. Rev. Lett.* **116**, 172302 (2016).
39. ATLAS Collab., *Measurement of multi-particle azimuthal correlations in pp, p+Pb and low-multiplicity Pb+Pb collisions with the ATLAS detector*, *Eur. Phys. J. C* **77**, 428 (2017).
40. CMS Collab., *Evidence for collectivity in pp collisions at the LHC*, *Phys. Lett. B* **765**, 193 (2017).
41. CMS Collab., *Multiplicity and transverse momentum dependence of two- and four-particle correlations in pPb and PbPb collisions*, *Phys. Lett. B* **724**, 213 (2013).
42. ALICE Collab., *Insight into particle production mechanisms via angular correlations of identified particles in pp collisions at  $\sqrt{s} = 7$  TeV*, *Eur. Phys.J. C* **77**, no.8, 569 (2017).
43. ATLAS Collab., *Two-particle Bose-Einstein correlations in pp collisions at  $\sqrt{s} = 0.9$  and 7 TeV measured with the ATLAS detector*, *Eur. Phys. J C* **75**, 466 (2015).
44. CMS Collab., *Measurement of Bose-Einstein Correlations in pp Collisions at  $\sqrt{s} = 0.9$  and 7 TeV*, *J. High Energy Phys.* **05**, 029 (2011).
45. UA1 Collab., *Bose-Einstein Correlations in  $\bar{p}p$  Interactions at  $\sqrt{s} = 0.2$  to 0.9 TeV*, *Phys. Lett. B* **226**, 410 (1989).
46. ATLAS Collab., *Femtoscopy with identified charged pions in proton-lead collisions at  $\sqrt{s} = 5.02$  TeV with ATLAS*, CERN-EP-2017-004, arXiv:1704.01621 [hep-ex].
47. LHCb Collab., *Bose-Einstein correlations of same-sign charged pions in the forward region in pp collisions at  $\sqrt{s} = 7$  TeV*, *J. High Energy Phys.* **1712** 025 (2017).
48. ALICE Collab., *Multipion Bose-Einstein correlations in pp,p-Pb, and Pb-Pb collisions at energies available at the CERN Large Hadron Collider*, *Phys. Rev. C* **93**, 054908 (2016).
49. S. Todorova-Nova, *Quantization of the QCD string with a helical structure*, *Phys. Rev. D* **89**, no.1, 015002 (2014).
50. B. Andersson et al., *Is there screwiness at the end of the QCD cascades?*, *J. High Energy Phys.* **9809**, 014 (1998).
51. ATLAS Collab., *Study of ordered hadron chains with the ATLAS detector*, *Phys. Rev. D* **96**, no.9, 092008 (2017).